

Ultrasensitive label-free optical recording of bioelectric potentials using dioxythiophene-based electrochromic polymers

Received: 12 January 2025

Accepted: 26 June 2025

Published online: 23 July 2025



Yuecheng Zhou^{1,2,9}, Erica Liu^{1,2}, Anna M. Österholm³, Austin L. Jones³, Pengwei Sun^{2,4}, Yang Yang^{1,2}, Ching-Ting Tsai^{1,2}, Tomasz Zaluska^{2,5}, Wei Zhang^{1,2}, Holger Müller^{6,7}, John R. Reynolds^{3,8} & Bianxiao Cui^{1,2}✉

Dioxythiophene-based polymers are electrochromic, effectively converting electric potentials into optical signals through voltage-dependent changes in absorption. The electrochromic property of these π -conjugated polymers can be harnessed to transform miniscule bioelectric signals, such as neuronal action potentials, into optical readouts. To enhance sensitivity, we investigated the impact of backbone and side-chain chemistry of dioxythiophene-based polymers. Among them, P(OE3)-E, a copolymer of oligoether-functionalized 3,4-propylenedioxythiophene with unsubstituted 3,4-ethylenedioxythiophene, exhibits the highest electrochromic sensitivity for optical bioelectric potential detection. A crucial factor in optimizing detection sensitivity is aligning the electric potential that triggers the sharpest optical transition in electrochromic polymers with the redox potential of the biological environment. Using P(OE3)-E thin films, we reliably detected field potentials from isolated rat hearts, extracellular action potentials of stem cell-derived cardiomyocytes, and spontaneous action potentials of dissociated rat hippocampal neurons. Our results achieved a detection sensitivity of $\sim 3.3 \mu\text{V}$ with sub-millisecond temporal resolution, matching that of traditional electrode-based recordings while eliminating the constraints of electrode patterning or placement. This work highlights the significant potential of π -conjugated polymers for advancing bioelectric detection technologies.

A distinct class of redox-active π -conjugated polymers, known as organic mixed ionic-electronic conductors, is capable of transporting ions and at the same time conducting electrons along the polymer chain^{1,2}. The coupled ionic-electronic transport capability of these polymers enables prominent applications ranging from energy storage and conversion^{3–6} to bioelectronics^{7–10}. In bioelectronics, π -conjugated

polymers are widely implemented as electrode materials due to their electronic conductivity, efficient ion-to-electron conversion, processability, and superb biocompatibility. These materials allow ions to penetrate the bulk of the polymer matrix and exhibit orders of magnitude lower impedance than flat metallic electrodes of similar area¹¹. Indeed, they have been used as electrode materials to detect local field

¹Department of Chemistry, Stanford University, Stanford, CA, USA. ²Wu Tsai Neurosciences Institute, Stanford University, Stanford, CA, USA. ³School of Chemistry and Biochemistry, Georgia Institute of Technology, Atlanta, GA, USA. ⁴Department of Radiology, Stanford University, Stanford, CA, USA.

⁵Department of Bioengineering, Stanford University, Stanford, CA, USA. ⁶Department of Physics, University of California, Berkeley, CA, USA. ⁷Molecular Biophysics and Integrated Bioimaging, Lawrence Berkeley National Laboratory, Berkeley, CA, USA. ⁸School of Materials Science and Engineering, Georgia Institute of Technology, Atlanta, GA, USA. ⁹Present address: Department of Materials Science and Engineering, The Grainger College of Engineering, University of Illinois Urbana-Champaign, Urbana, IL, USA. ✉e-mail: bcui@stanford.edu

potentials from surface cortical neurons¹², map the electrical activity of porcine and rabbit hearts⁸, record action potentials from heart muscle cells¹⁰, and fabricate organic neuromorphic devices with synaptic plasticity mediated by neurotransmitters that mimic biological synaptic behavior⁹.

Although π -conjugated polymers are primarily known for their electrical conductivity, these polymers also possess an interesting optical property—electrochromism, referring to materials changing color (or light absorbance) in response to an applied voltage¹³. This electrochromic property results from distinct electronic transitions in the polymer's reduced and oxidized states, controlled by the external potential. We recently demonstrated that the voltage-dependent absorbance of poly(3,4-ethylenedioxythiophene) (PEDOT), the most widely used conductive polymer, can be harnessed to convert bioelectric signals into optical readouts^{14,15}. The ElectroChromic Optical Recording (ECORE) technique enables the detection of bioelectric signals from cells by measuring the change in light absorption of electrochromic polymers.

Bioelectric signals are essential for a wide range of physiological functions, including neuronal activity, muscle contraction, and the rhythmic beating of the heart. Key cells in our body, such as neurons in our brain and cardiomyocytes in our heart, rely on bioelectric signals to transmit signals and coordinate their functions. Accurately detecting these bioelectric signals is critical for understanding their underlying mechanisms, developing diagnostic tools, and assessing treatment strategies. Compared to traditional electrode-based detection methods, optical recording offers spatial flexibility and imaging feasibility. Unlike fluorescence-based voltage sensing techniques, ECORE is an optical recording technique that does not require the incorporation of fluorescent reporter molecules into cells and thus does not suffer from photobleaching or phototoxicity. However, the extracellular bioelectric signals are often very weak, typically in the range of tens of microvolts, resulting in a very subtle color change (the signal) in ECORE recordings. Despite the recent development of advanced optical techniques¹⁴, the limited sensitivity remains a significant challenge, especially when it comes to detecting spontaneous, irregular, and fast-spiking neuronal activities. Overcoming this challenge is crucial for advancing ECORE into a reliable and effective tool for electrophysiology.

In this work, we showed that π -conjugated polymers with varying backbone and side-chain structures can drastically enhance the electrochromic contrast and the detection sensitivity of ECORE. Specifically, we explored the electrochromic contrast of four different types of π -conjugated polymers in response to bioelectric signals: (i) electropolymerized PEDOT directly from monomer EDOT, (ii) solution-polymerized and spin-coated PEDOT:PSS, (iii) P(OE3)-D¹⁶, an alternating copolymer of oligoether functionalized 3,4-propylenedioxythiophene (ProDOT) and 2,2-dimethyl ProDOT, and (iv) P(OE3)-E¹⁷, an alternating copolymer of oligoether functionalized ProDOT and unsubstituted EDOT. We found that, in cell culture conditions, the electrochromic color contrast of P(OE3)-E significantly surpasses the other polymers. Using P(OE3)-E, we reliably detected spontaneous field potentials from rat hearts, action potentials from human induced pluripotent stem cell-derived cardiomyocytes (hiPSC-cardiomyocytes), and rat hippocampal neurons. In this study, we achieved a remarkable detection sensitivity of $-3.3\ \mu\text{V}$ using P(OE3)-E, which does not photobleach or induce phototoxicity, and thus enables durable, label-free, and spatially-versatile detection of bioelectric signals by light. We also achieved a detection temporal resolution with a recording bandwidth of 10 kHz and clearly distinguished the neuronal burst firing events as fast as 93 Hz. This work underscores the opportunities of π -conjugated polymers for non-invasive, high-resolution, and spatially flexible monitoring of bioelectric signals.

Results

Characterization of electrochromic polymer thin films

While previous ECORE studies successfully used electropolymerized PEDOT:PSS thin films as the sensing material, PEDOT demonstrated a relatively small voltage-dependent spectral shift and thus a limited signal strength. PEDOT is not soluble in aqueous solutions on its own, but thin films can be formed from colloidal dispersions when mixed with the ionic polymer poly(styrene sulfonate) (PSS), or through electropolymerization in the presence of PSS or other salts. PProDOT and copolymers with varied side-chain substituents have been shown to exhibit notably higher electrochromic optical contrast than PEDOT^{16–19}. For ECORE applications, it is crucial that the polymers are biocompatible, easily processable, and exhibit a high electrochromic contrast in cell culture conditions¹⁴. These requirements motivated us to choose P(OE3)-D, a ProDOT polymer, and P(OE3)-E, a ProDOT-EDOT copolymer (Fig. 1a). Both polymers exhibit large voltage-dependent spectral shifts, high redox stabilities due to the protection of 3,4 positions on the thiophene ring, and low oxidation potentials due to the di-substitution of π -donating oxygen atoms compared to other thiophene-based polymer analogs^{17,19}. We systematically compared the electrochromic sensitivity of electropolymerized PEDOT:PSS (noted as PEDOT-epoly), spin-coated PEDOT:PSS (noted as PEDOT-spin), spin-coated P(OE3)-D, and spin-coated P(OE3)-E thin films for ECORE applications (Fig. 1a).

Atomic Force Microscopy (AFM) imaging shows that the PEDOT-spin thin film has a surface roughness of 2.2 nm, while PEDOT-epoly exhibits, not unexpectedly, a significantly rougher surface at 9.3 nm with lateral granular domains between 50 nm and 100 nm. On the other hand, P(OE3)-D and P(OE3)-E have polar oligo-ether side chains that grant them molecular solubility in common organic solvents and solution processability²⁰. AFM imaging shows that spin-coated P(OE3)-E and P(OE3)-D form smooth films with a surface roughness of 0.7 nm with no lateral granular domains (Fig. 1b). A smooth surface is expected to enhance ECORE performance by reducing light scattering at the granular interface. When subjected to different applied voltages at $-300\ \text{mV}$, $0\ \text{mV}$ and $+300\ \text{mV}$ with respect to an Ag/AgCl reference electrode in HEPES buffered Tyrode's solution, $\sim 70\ \text{nm}$ films made of all four materials exhibit clear electrochromism and visible color changes (Fig. 1c). The PEDOT-epoly film appears purple in the reduced (dedoped) state and blue in the oxidized (doped) state. The PEDOT-spin film exhibits weak absorption and poor color contrast at this film thickness (Supplementary Fig. 1b), but it shows clearer electrochromic color contrast, from light blue to lighter blue, with thicker films (Fig. 1c). The P(OE3)-D film appears dark purple in the reduced state and transitions to light pink in the oxidized state. The P(OE3)-E film shows a strong color contrast from dark blue in the reduced state to almost transparent in the oxidized state.

To quantify the electrochromic behavior of the four polymer films, we measured their Visible-Near Infrared (Vis-NIR) absorption when the applied potential was systematically changed from $-600\ \text{mV}$ to $+600\ \text{mV}$ with respect to an Ag/AgCl reference electrode in HEPES buffered Tyrode's salt solution (Fig. 1d, "Methods"). The voltage range is sufficient to drive all materials into the reduced (dedoped) or oxidized (doped) states. Due to the poor absorption of PEDOT-spin film, a thick film was used in the Vis-NIR measurement. Each spectrum shows a pronounced absorbance peak in the reduced state originating from the π - π^* transition, 523 nm for PEDOT-epoly, 658 nm for PEDOT-spin, 572 nm for P(OE3)-D, and 608 nm for P(OE3)-E. PEDOT-epoly shows a blue-shifted peak compared to PEDOT-spin, which is attributed to the formation of shorter polymer chains and thus an increased π - π^* energy gap^{21,22}. As the applied potential increases, the peak height corresponding to the reduced state gradually decreases and is accompanied by the rise of a much-red-shifted peak, corresponding to the charge carrier absorption originating from the oxidized states.

Figure 1e shows the normalized Vis-NIR absorbance change (see “Methods”) for all polymer films at 561 nm, the laser wavelength used in the ECORE experiments. P(OE3)-E and P(OE3)-D films show substantially larger absorbance changes than PEDOT-epoly and PEDOT-spin films at 561 nm. The transition potential, corresponding to the sharpest absorbance change, emerges between -100 mV and $+100$ mV for P(OE3)-E, and between $+300$ mV and $+450$ mV for P(OE3)-D, matching the potential window where the two polymers transition from insulating (reduced) to conductive (oxidized) state¹⁷. The corresponding transition potentials for PEDOT-epoly and PEDOT-spin emerge at lower potentials, i.e., between -200 mV and -50 mV and between -300 mV and -150 mV, respectively. This transition potential is important in biological applications as we show later.

The density of electroactive sites in polymer films is expected to positively affect electrochromic responses. We estimated the density of electroactive sites of each polymer film from their reductive currents in cyclic voltammograms (Fig. 1f and Supplementary Fig. 2). We note the anodic limit of all polymers ranges between 0.6 and 0.7 V. Hence, we used the reductive peak current below 0.6 V when

estimating the electroactive site concentration with the assumption that one charge interacts with one electroactive site in the polymer (Supplementary Text 2). We found that PEDOT-epoly thin film has the highest active site concentration ($2.0 \pm 0.1 \mu\text{mol}/\text{mm}^2$) while PEDOT-spin thin film has the lowest at $0.5 \pm 0.1 \mu\text{mol}/\text{mm}^2$. This is likely due to a low PEDOT:PSS ratio and a low mass density of commercial PEDOT:PSS dispersions compared to electropolymerized PEDOT:PSS, and is consistent with previously reported findings in literature²³. P(OE3)-D and P(OE3)-E thin films have intermediate active site concentrations at $0.9 \pm 0.1 \mu\text{mol}/\text{mm}^2$ and $0.6 \pm 0.2 \mu\text{mol}/\text{mm}^2$, respectively (Fig. 1g).

ECORE responses of PProDOT and PEDOT films under cell-free conditions

To characterize the performance of π -conjugated polymer thin films in ECORE, we built an optical detection setup consisting of a prism-coupled total internal reflectance platform and differential photo-detection (Fig. 2a), as previously described^{14,15}. A 561 nm laser is used as the probing light source. When a train of 1 mV, 1 Hz squarewave potential is applied to the film, it results in a clear optical response,

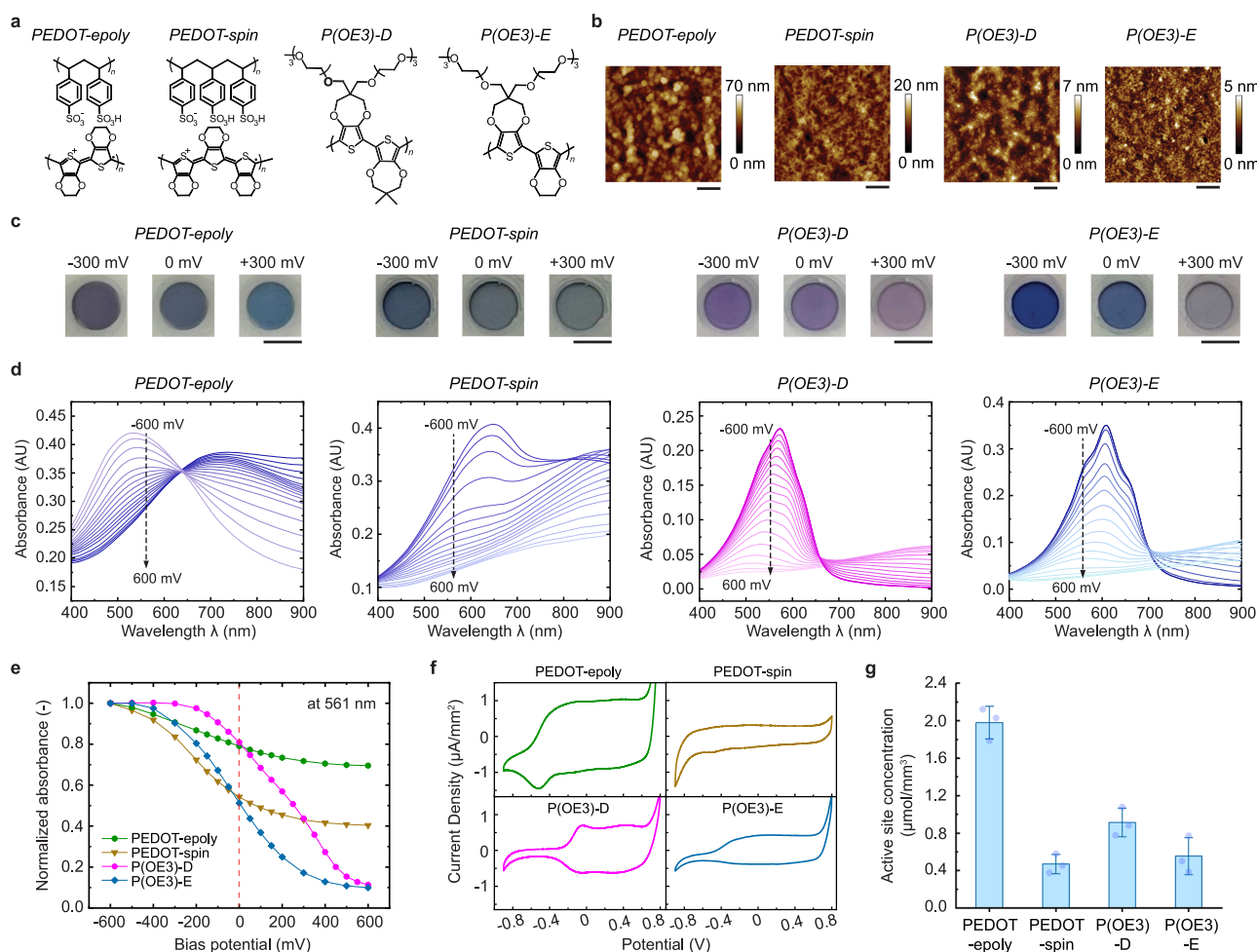


Fig. 1 | Materials characterization of PProDOT and PEDOT polymer thin films. **a** Repeat unit structures of electropolymerized PEDOT:PSS (PEDOT-epoly), commercial PEDOT:PSS dispersions (PEDOT-spin), oligoether functionalized ProDOT copolymerized with 2,2-dimethyl ProDOT [P(OE3)-D], and oligoether functionalized ProDOT copolymerized with unsubstituted EDOT [P(OE3)-E]. **b** Atomic Force Microscopy (AFM) images of PEDOT-epoly, PEDOT-spin, P(OE3)-D, and P(OE3)-E thin films. Scale bar = 200 nm. Each experiment was repeated independently with similar results at least 3 times. **c** Color change of PEDOT-epoly, PEDOT-spin, P(OE3)-D, and P(OE3)-E thin films at -300 mV, 0 mV, and $+300$ mV. Scale bar = 5 mm. **d** Visible-near infrared (Vis-NIR) spectroelectrochemistry of PEDOT-epoly,

PEDOT-spin, P(OE3)-D and P(OE3)-E thin films from -600 mV to $+600$ mV in HEPES buffered Tyrode's salt solution. **e** Normalized Vis-NIR absorbance change of PEDOT-epoly (green hexagon), PEDOT-spin (yellow triangle), P(OE3)-D (pink circle), and P(OE3)-E (blue diamond) films at 561 nm. The dashed line indicates zero bias potential. **f** Cyclic voltammograms of different polymer films measured at a scan rate of 200 mV/s on ITO glasses in HEPES buffered Tyrode's salt solution. The y-axis is scaled to focus on the faradaic current below 0.7 V. **g** Active sites concentration in different polymer thin films estimated from the reductive current of cyclic voltammetry. Data are presented as mean \pm SD; $n = 3$ polymer films.

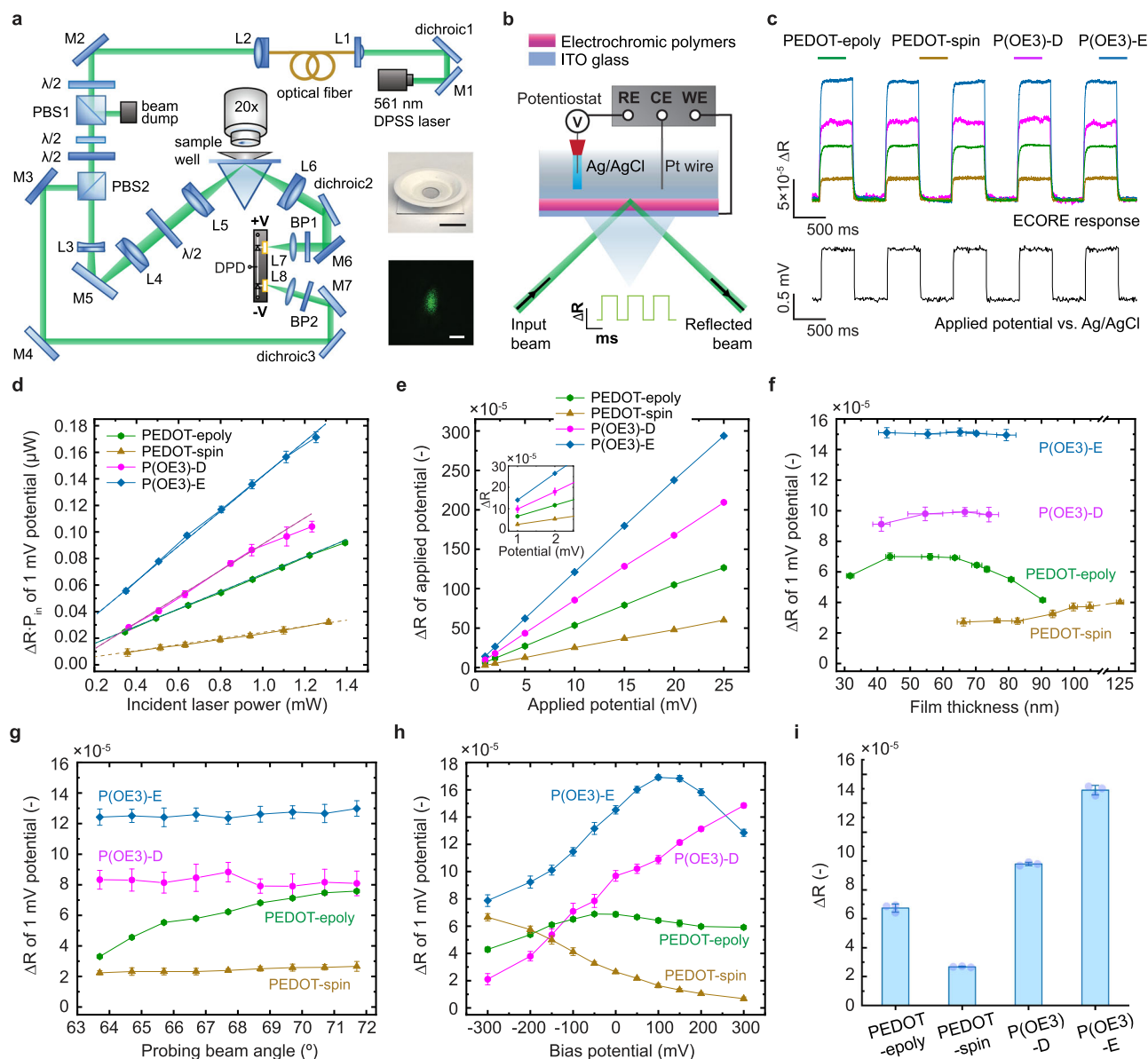


Fig. 2 | Characterization of ECORE sensitivity using PProDOT and PEDOT polymer thin films. **a** Optical setup of ECORE using prism-coupled total internal reflection. M mirror, L lens, $\lambda/2$: half-wave plate, PBS polarizing beam splitter, BP bandpass filter, DPD differential photodetector, DPSS laser diode-pumped solid-state laser. Inset 1: photo of a cell culture device for ECORE measurement. Scale bar = 1 cm. Inset 2: The probing laser of 561 nm is focused to the prism with a spot size of -25 μm (diameter at $1/e^2$ intensity). Images are false-colored and scale bar = 25 μm . **b** Schematic of the ECORE setup. A 561 nm probing laser is total-internally reflected at the interface of polymer and electrolyte solution. The electrochromic polymer thin film is modulated using a potentiostat based on a three-electrode configuration. RE reference electrode, CE counter electrode, WE working electrode. **c** Measured reflectance change, ΔR , of the four polymer thin films (top

panel) when a train of 1 mV, 1 Hz squarewave potential is applied (bottom panel). **d** Measured reflectance change, $\Delta R \cdot P_{in}$ (in microwatts), of different polymers as a function of incident laser beam power. **e** Measured reflectance change, ΔR , of different polymer films in response to 1 mV, 1 Hz squarewave potentials with respect to (f) different polymer film thicknesses, **g** different probing beam incident angles, and (h) under different bias potentials. Data are presented as mean \pm SD; $n = 55$ squarewave cycles; PEDOT-epoly, PEDOT-spin, P(OE3)-D, and P(OE3)-E films are denoted as green hexagon, yellow triangle, pink circle, and blue diamond, respectively in (d–h). **i** Comparison of the reflectance change, ΔR , of the four polymer thin films in response to 1 mV, 1 Hz squarewave potential at zero bias. Data are presented as mean \pm SD; $n = 3$ polymer films.

measured by the film reflectance change, ΔR (Fig. 2b, c). The reflectance, R , of the four polymers is shown in Supplementary Fig. 4a. In our experiment, the photodetector measures the product of ΔR and incident laser beam power, $\Delta R \cdot P_{in}$. We find that $\Delta R \cdot P_{in}$ for all polymer films in response to 1 mV, 1 Hz squarewave potential with respect to an Ag/AgCl reference electrode is linearly dependent on the incident laser beam power from 0.3 mW to 1.2 mW (Fig. 2d). Hence, we normalized $\Delta R \cdot P_{in}$ with respect to the incident laser beam intensity, P_{in} , and used the film reflectance ΔR as a direct comparison between different materials (see “Methods”). The ΔR for all polymer films is also linearly

proportional to the magnitude of applied potentials up to 25 mV (Fig. 2e). This allows quantitative conversion of ΔR to voltage if each film is calibrated.

We then characterized the influence of polymer film thickness on the ECORE performance, i.e., ΔR of 1 mV potential. For all experiments, a train of 1 mV, 1 Hz squarewave potentials with respect to an Ag/AgCl reference electrode was applied to the polymer films and the detection sensitivity in terms of ΔR was measured. As shown in Fig. 2f, PEDOT-epoly films show stable detection sensitivities between 43 and 64 nm and decrease with thicker film. PEDOT-spin films show small but stable

detection sensitivity from 66 to 83 nm and the sensitivity increases for thicker films. The detection sensitivity of P(OE3)-D films gradually increases from 41 to 55 nm and remains stable. The detection sensitivity of P(OE3)-E films is the highest among the four and remains stable between 40 and 80 nm. Because cells will be cultured on top of the thin films and our optical detection scheme is based on total-internal-reflection, where the evanescent wave decreases exponentially from the interface, we choose ~60 nm film thickness for all polymers.

Although the Ecore performance of PEDOT-epoly film is sensitive to the incident angle of the probing beam, we found that the performances of PEDOT-spin, P(OE3)-D, and P(OE3)-E thin films are rather independent of the incident angle (Fig. 2g). This angle insensitivity is beneficial for Ecore measurement as it increases the angle tolerance and the optical stability. We set the incident angle at -68.5° to maintain good sensitivity for all polymers for a comparison.

π -conjugated polymers undergo redox transitions at different voltages. To understand the influence of a polymer film's redox states on their Ecore detection sensitivity, we biased the film with different potentials and applied 1 mV, 1 Hz squarewave potential on top of the biasing potential. As shown in Fig. 2h, the detection sensitivity of PEDOT-epoly film peaks at -50 mV, whereas the detection sensitivity of the PEDOT-spin film decreases monotonically with the increasing potential due to it having the lowest oxidation potential of the four. The detection sensitivity of P(OE3)-D film is minimal below -200 mV and starts to increase drastically with increasing potential. The detection sensitivity of P(OE3)-E film increases and peaks at 100 mV before decreasing with the applied potential. Nevertheless, it maintains the highest detection sensitivity from -200 to 200 mV among all polymers. These data agree with the Vis-NIR data shown in Fig. 1e and show that the transition potential (corresponding to the sharpest absorbance change) increases in the order of PEDOT-spin (<-200 mV), PEDOT-epoly (-50 mV), P(OE3)-E ($+100$ mV), and P(OE3)-D ($>+300$ mV). As shown later, the oxidation transition potential is one of the most crucial parameters in bioelectronic applications where no bias potential is applied.

For thin films with an active area of 28.3 mm^2 , the 10–90% rise time of the Ecore optical response to 1 mV squarewave potential is measured to be 43.2 ± 2.1 ms for PEDOT-epoly, 22.6 ± 5.9 ms for PEDOT-spin, 38 ± 6 ms for P(OE3)-D, and 24.7 ± 0.8 ms for P(OE3)-E thin films (Supplementary Fig. 4b). We noted that the temporal response of polymer thin films scales with the square root of the sensing area¹⁵, which is a characteristic of the resistor-capacitor circuit model for microelectrodes²⁴. For a cell with an area of $\sim 400\text{ }\mu\text{m}^2$, we expect the temporal response time of all polymer films to be less than 0.2 ms. Therefore, all four polymers provide the necessary sub-millisecond temporal resolution for bioelectric signal recordings (Supplementary Text 4).

With a 60-nm film thickness, a -68.5° laser incident angle, and a zero-bias voltage for all polymers, we compared the Ecore performance ΔR in response to the voltage modulation of a train of 1 mV, 1 Hz squarewave potentials. Compared to PEDOT-epoly ($\Delta R = 6.7 \times 10^{-5} \pm 0.3 \times 10^{-5}$) used in previous Ecore studies^{14,15}, PEDOT-spin shows 61% reduction in sensitivity, while P(OE3)-D ($\Delta R = 9.8 \times 10^{-5} \pm 0.1 \times 10^{-5}$) shows 43% enhancement and P(OE3)-E ($\Delta R = 14.9 \times 10^{-5} \pm 0.3 \times 10^{-5}$) shows ~110% enhancement (Fig. 2i). The recording baseline noise typically has a ΔR of -0.05×10^{-5} . P(OE3)-E shows a signal-to-noise ratio of ~300 in response to a 1 mV applied potential, corresponding to a detection sensitivity of $-3.3\text{ }\mu\text{V}$. In cell-free characterization studies, the redox states of the polymers were controlled using a three-electrode potentiostat. In our following bioelectric measurements, all experiments were conducted under open-circuit with no electrode in the solution. In these studies, the redox states of different polymer films were determined by the open-circuit

potential, E_{oc} , which are dependent on the biological systems they are interfaced with.

Ecore recording of electric potentials from embryonic rat hearts

We examined the Ecore performance of different polymer films in recording field potentials from embryonic rat hearts. The rat hearts were isolated from day 18 rat embryos (E18) and cultured in vitro before measurements (see “Methods” and Fig. 3b). These embryonic rat hearts maintain rhythmic electric potentials and mechanical contractions up to two months of culture in vitro. For each measurement, a single rat heart was directly transferred to the polymer film (see “Methods”). The laser beam was steered to the heart-polymer interface and recordings were performed at room temperature (Fig. 3a). Three rat hearts on three independent films were measured for each polymer. Typical recording traces using PEDOT-epoly, PEDOT-spin, P(OE3)-D and P(OE3)-E thin films are shown in Fig. 3c–f. Bioelectric signals from rat hearts appear as periodic sharp spikes. The zoomed-in view (red dashed box) shows electric signals as single-phasic or bi-phasic spikes. The shape of the electric signal shows great variability even on the same type of polymer film, likely due to measuring different heart locations in each measurement (see additional traces in Supplementary Fig. 5). Immediately following the fast field potential spike is typically the slow baseline shift due to the mechanical contraction of the heart, known as the cardiac excitation-contraction coupling²⁵. The rise time of single-phasic or bi-phasic field potential spikes was measured for all four materials (see “Methods” and Supplementary Fig. 6). The field potentials measured on all four polymers show average timescales between 3 and 6 ms. This is within the range of extracellular potential spikes from hearts that correspond to the initial fast depolarization phase due to the opening of the Na^+ ion channel^{26–28}.

The spike magnitude of the recorded rat heart field potentials using different polymers is summarized in Fig. 3g. P(OE3)-E thin film shows the highest recording sensitivity ($\Delta R = 6.4 \times 10^{-5} \pm 1 \times 10^{-5}$, $n = 3$) followed by P(OE3)-D thin film ($\Delta R = 5.3 \times 10^{-5} \pm 1 \times 10^{-5}$, $n = 3$) and PEDOT-epoly thin film ($\Delta R = 4.5 \times 10^{-5} \pm 0.5 \times 10^{-5}$, $n = 3$). PEDOT-spin shows the lowest sensitivity ($\Delta R = 0.6 \times 10^{-5}$, $n = 3$). It is important to note that bioelectric recordings were performed under open-circuit conditions. The open-circuit potential, E_{oc} , of the polymer films determines their respective equilibrium redox states and regulates their recording sensitivities. The E_{oc} of the polymer films is influenced by the chemical compositions of the cell/tissue culture medium. We experimentally measured E_{oc} for each polymer film under the recording conditions for rat hearts (see “Methods”). The measured E_{oc} s are 77.5 mV for PEDOT-epoly, 242.5 mV for PEDOT-spin, 177.5 mV for P(OE3)-D and 122.2 mV for P(OE3)-E with respect to the Ag/AgCl reference electrode (Supplementary Table 1) and P(OE3)-E shows the highest sensitivity for rat heart recording.

Figure 3h shows a prolonged recording trace of rat heart field potentials for 18 min at 10 kHz recording frequency using a spin-coated P(OE3)-E thin film. The zoomed-in snapshots at different timestamps resolved the millisecond field potential spike (Fig. 3i). The amplitude of the optical signal remains stable without time-dependent degradation over the long recording period, highlighting the non-perturbative nature of Ecore. Variations in the beating frequency are common to cultured rat hearts. Therefore, P(OE3)-E affords excellent signal quality and stability for bioelectric optical recording.

Ecore recording and pharmacological study of hiPSC-cardiomyocyte action potentials

Moving beyond recording field potentials, we examined the use of four polymers in recording extracellular action potentials from single human-induced pluripotent stem cell-derived cardiomyocytes (hiPSC-cardiomyocytes). These cardiomyocytes are large cells between 50 and 100 μm in diameter, so we can achieve single-cell resolution using

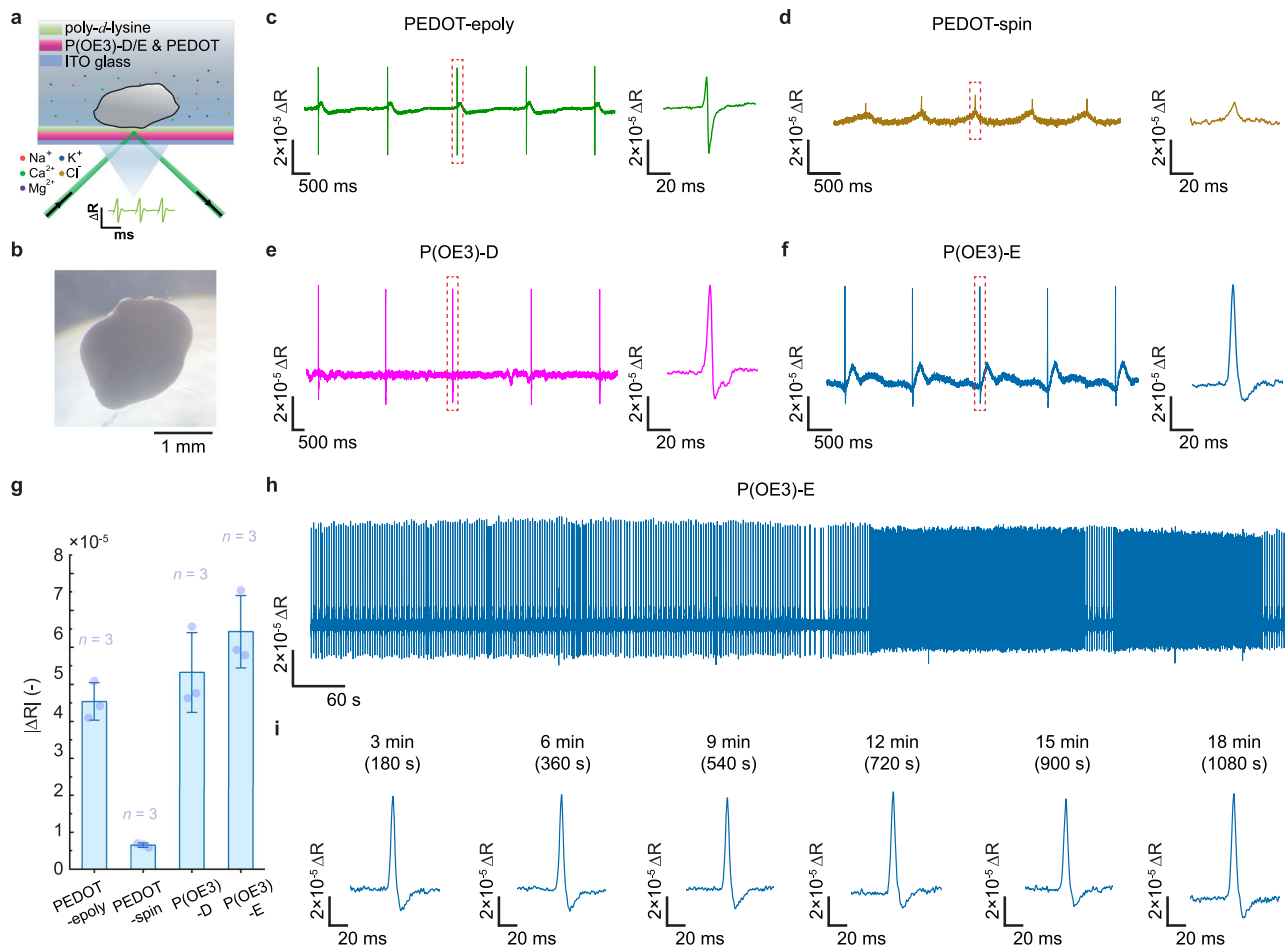


Fig. 3 | ECORE recording of isolated rat heart field potential using polymer thin films. **a** Schematic drawing of an isolated embryonic rat heart placed on top of electrochromic polymer thin films. The probing laser is focused at the tissue-polymer interface and is total-internally reflected. The reflected light is sensitive to the spectral shift of the polymer films induced by the heart field potentials. **b** Optical micrograph of a cultured heart from day 18 rat embryos (E18). The experiment was repeated independently with similar results at least five times.

ECORE recording trace of a cultured E18 rat heart using **c** PEDOT-epoly thin film, **d** PEDOT-spin thin film, **e** P(OE3)-D thin film, and **f** P(OE3)-E thin film. **g** Comparison of the recording performance for heart field potentials in terms of reflectance change, ΔR , using four polymer thin films. Data are presented as mean \pm SD; $n = 3$ hearts. **h** An 18-min recording trace at 10 kHz recording frequency of an E18 rat heart. **i** Zoomed-in traces at 3, 6, 9, 12, 15, and 18 min show that the optical signal remains stable over the long recording period.

ECORE ($\sim 25 \mu\text{m}$ probing beam spot) (Figs. 4a and 2a and “Methods”). hiPSC-cardiomyocytes were cultured on polymer thin films and ECORE recordings were performed a week after cell seeding when cardiomyocytes formed a confluent monolayer and beat synchronously (see “Methods” and Fig. 4b). Representative recording traces of ΔR are shown for cells cultured on thin films of PEDOT-epoly (Fig. 4c), PEDOT-spin (Fig. 4d), P(OE3)-D (Fig. 4e) and P(OE3)-E (Fig. 4f). All traces show large and periodic peaks with a peak duration of 600–1400 ms. These are not electric signals but arise from the periodic mechanical contraction of cardiomyocytes that modulate the light reflection at the cell-polymer interface. The contraction signals for cultured hiPSC-cardiomyocytes are much stronger than rat hearts because these cells were cultured on and tightly adhere to the polymer films while rat hearts were gently placed on top without adhering to the polymer films.

The extracellular action potentials of hiPSC-cardiomyocytes appear as sharp spikes before the start of mechanical contraction (red dashed box in Fig. 4c–f). A zoomed-in view shows single-phasic spikes with a rise or drop time of ~ 1.8 ms (see “Methods” and Supplementary Fig. 7a–c), which corresponds to the fast depolarization phase of intracellular action potential resulting from the opening of the Na^+ channel¹⁴. Quantifications of ΔR for extracellular action potentials over many hiPSC cultures ($n \geq 15$ for each polymer film) are shown in Fig. 4g.

P(OE3)-E film shows the highest detection sensitivity ($\Delta R = 4.2 \times 10^{-5} \pm 1.2 \times 10^{-5}$, $n = 24$) followed by electropolymerized PEDOT film ($\Delta R = 1.3 \times 10^{-5} \pm 0.4 \times 10^{-5}$, $n = 20$) and PEDOT-spin film ($\Delta R = 0.6 \times 10^{-5} \pm 0.5 \times 10^{-5}$, $n = 15$).

A noteworthy observation is that electric signals from hiPSC-cardiomyocytes are not-detected or barely detectable P(OE3)-D films ($\Delta R = 0.2 \times 10^{-5} \pm 0.2 \times 10^{-5}$, $n = 17$). To understand why P(OE3)-D films measure large electric signals from rat hearts but not from hiPSC-cardiomyocytes, we measured the open-circuit potential for four polymer films after exposure to the cell culture medium for 7 days in the incubator. The E_{oc} for all films are less than zero, -61.2 mV for PEDOT-epoly, -26.6 mV for PEDOT-spin, -7.7 mV for P(OE3)-D, and -38.9 mV for P(OE3)-E. These values are lower compared to E_{ocs} of the same films at the rat heart recording conditions, likely due to the presence of reductive compounds in the cell culture medium¹⁴. The electrochromic sensitivity of P(OE3)-D decreases with applied voltage (see Fig. 2h). Nevertheless, E_{oc} alone cannot fully explain the poor sensitivity of P(OE3)-D film in recording hiPSC-cardiomyocytes. These measurements highlight the importance of considering specifics of biological applications in the selection of π -conjugated polymers in bioelectronics.

After applying a 2 Hz, 1st-order Butterworth high-pass filter to remove the slow mechanical contraction (see “Methods”), a prolonged

recording trace of a single hiPSC-cardiomyocyte on a P(OE3)-E thin film is shown in Fig. 4h. The recorded action potential achieved an average ΔR of $5.5 \times 10^{-5} \pm 0.4 \times 10^{-5}$ over 510 s. Snapshots of action potentials at different timestamps show stable ΔR over the 510-s period (Fig. 4i). In addition, we recorded hiPSC-cardiomyocytes from the same P(OE3)-E film device repeatedly for over 5 weeks (37 days) (Supplementary Fig. 7d–h). The detection sensitivity of P(OE3)-E remains excellent (ΔR ranges between 3.6×10^{-5} and 4.8×10^{-5}) over the 5-week duration (Supplementary Fig. 7i).

To examine whether P(OE3)-E-based ECORE can detect changes in cardiac action potentials induced by ion channel blockers, we measured the pharmacological effects of quinidine. Quinidine is a Na^+ and Ca^{2+} channel blocker that slows down the depolarization phase of cardiomyocyte intracellular action potential (Fig. 4j, k)²⁹. Two doses of quinidine were sequentially added to the cardiomyocyte culture while the culture was being recorded. The first dose was added around 126 s (final concentration of $1 \mu\text{M}$) and the second dose added ~ 669 s (final concentration of $4.6 \mu\text{M}$) (Fig. 4l). The ECORE recording trace shows a slight decrease in the ΔR amplitude after the first dose and a drastic decrease after the second dose (Fig. 4l, m and Supplementary Fig. 7j). The drop time of the action potential spikes shows negligible change under $1 \mu\text{M}$ quinidine, but drastically slows down with after $4.6 \mu\text{M}$ quinidine (Fig. 4n and Supplementary Fig. 7j). Therefore, the addition of high dose quinidine resulted in prolonged spike duration, the decrease of spike amplitude, and the ultimate disappearance of action potential signals, expected effects for Na^+ and Ca^{2+} channel blockers³⁰.

ECORE recording of neuronal action potentials

Extracellular action potentials of neurons are smaller in amplitude and faster in time than that of cardiomyocytes. To determine whether ECORE can reliably detect neuronal action potentials, we chose P(OE3)-E for its superior sensitivity. Dissociated hippocampal neurons from day 18 rat embryos (E18) were cultured on the P(OE3)-E thin films and were maintained in vitro for up to 5 weeks (see “Methods”). We performed ECORE recordings 2–3 weeks after cell seeding on the P(OE3)-E thin film (Fig. 5a) when dissociated neurons form interconnected networks (see “Methods” and Fig. 5b). The neuron soma is 20–30 μm in diameter, which is approximately the size of the probing laser ($\sim 25 \mu\text{m}$). Figure 5c shows the recording trace from a single neuron 23 days after cell seeding. Spontaneous neuronal action potentials appear as millisecond spikes (1st red arrow in Fig. 5c) that are resolved with a high temporal resolution at 10 kHz recording frequency (Fig. 5d). These spikes show a typical waveform of neuronal extracellular action potential near the soma³¹, with an average firing frequency of 2.4 Hz and many activity bursts³². Zoomed-in plots of two such bursts (2nd and 3rd red arrow in Fig. 5c) are shown in Fig. 5e, f. In such bursts, neighboring spikes with intervals as short as 11 ms (corresponding to 93 Hz) can be resolved.

Cultured hippocampal neurons mature over time and usually begin to exhibit some action potentials after 2 weeks in culture (day 14) and the firing frequency with time³³. Our optical recordings of day-17 neurons show a lower average firing frequency of 0.8 Hz (Fig. 5h). At day-16, cultured hippocampal neurons exhibited sparse and sporadic action potentials. To stimulate neuronal firing activities, we stimulated them with carbachol, an acetylcholine receptor^{34,35} agonist that increases neuronal activities. Indeed, before carbachol treatment, ECORE recording trace shows that the neuron is mostly silent (Fig. 5i). After adding $27.5 \mu\text{M}$ carbachol, the neurons show firing bursts with an average frequency of 1.3 Hz. The spike number and amplitude gradually reduced over time, which is expected for hippocampal neurons after carbachol stimulation³⁶. This confirmed the detected electrical spikes are neuronal extracellular action potentials.

The extracellular action potential of neurons is significantly smaller in magnitude than the isolated rat heart and hiPSC-cardiomyocyte extracellular action potentials. The average ΔR of neuronal extracellular action potential ($\Delta R = 0.6 \times 10^{-5} \pm 0.3 \times 10^{-5}$, $n = 9$, $E_{\text{oc}} = -44.9 \text{ mV}$) is $\sim 1/7$ of the extracellular action potential of hiPSC cardiomyocytes ($\Delta R = 4.2 \times 10^{-5} \pm 1.2 \times 10^{-5}$), and $\sim 1/10$ of the extracellular action potential of cultured rat heart ($\Delta R = 6.4 \times 10^{-5} \pm 1 \times 10^{-5}$) (Fig. 5g). All the identified neuronal action potential spikes in Fig. 5c, h, i are on the order of 1 ms (Supplementary Fig. 8), which are faster than the action potential spikes of hiPSC-cardiomyocytes ($\sim 1.8 \text{ ms}$) and cultured rat heart (3–6 ms). Nevertheless, the rapid and reversible redox property of P(OE3)-E polymer and its high electrochromic sensitivity enable reliable detection of the signature burst firing activity of dissociated hippocampal neuronal networks across a wide frequency range without data averaging.

Discussion

Optical recording of bioelectric potentials possesses unique advantages compared to electrode-based recording methods such as high spatial flexibility in selecting specific cells of interest, high spatial resolution for potential subcellular recording, and imaging capability³⁷. The fundamental challenge of optical electrophysiology is to convert bioelectric potentials into stable optical signals. Over the last decade, the development of voltage-dependent fluorescent molecules and proteins has significantly advanced the capability of optical recording and has enabled optical electrophysiology in cells³⁸, tissue³⁹, and live animals⁴⁰. Nevertheless, fluorescent probes suffer from low signal, photobleaching, and phototoxicity that could limit the recording duration or recording frequency.

ECORE leverages dioxythiophene-based electrochromic polymer thin films that convert bioelectric potentials into optical readouts via voltage-dependent reflectance change, rather than fluorescence. This is the key reason why ECORE does not suffer from photobleaching and allows us to use much lower laser power than that needed to excite fluorescence molecules. Furthermore, the electrochromic polymer film residing outside the cell does not induce phototoxicity, which is largely due to lipid oxidation by excited fluorescent molecules that are incorporated into the cell membrane or cytosol.

This work investigated the influence of polymer backbone structures on the ECORE performance by comparing electropolymerized and spin-coated PEDOT (backbone composed of EDOT only), spin-coated P(OE3)-D (backbone composed of ProDOT only), and spin-coated P(OE3)-E (backbone composed of both ProDOT and EDOT) thin films. Among the four polymers, P(OE3)-E exhibits the strongest electrochromic contrast with a highly reversible redox behavior and shows the highest sensitivity to bioelectric potentials. Both the choice of backbone and side chain play a critical role in contributing to the high electrochromic sensitivity. For P(OE3)-E, the reduced ring size of EDOT relative to ProDOT planarizes the monomer unit and enhances the π -donation of electron lone-pairs into the thiophene ring⁴¹. Therefore, P(OE3)-E shows smaller π – π stacking distance than P(OE3)-D, which increases molecular overlap and facilitates carrier delocalization and interchain charge transport⁴⁹. As a result, the P(OE3)-E backbone allows low oxidation potential, where the largest electrochromic change is matched with typical bioelectric signals^{17,18}. The polar side chains further allow aqueous compatibility of P(OE3)-E by coordinating ions under biological conditions. Additionally, the oligoether side chains of P(OE3)-E enhance performance by increasing polymer polarity, which promotes aqueous and biological electrolyte compatibility, water swelling of the polymer, and ion coordination (Na^+ under biological conditions).

This work demonstrates that P(OE3)-E significantly enhances the sensitivity and durability of ECORE, enabling long-term, label-free optical recordings of both cardiac and neuronal action potentials with

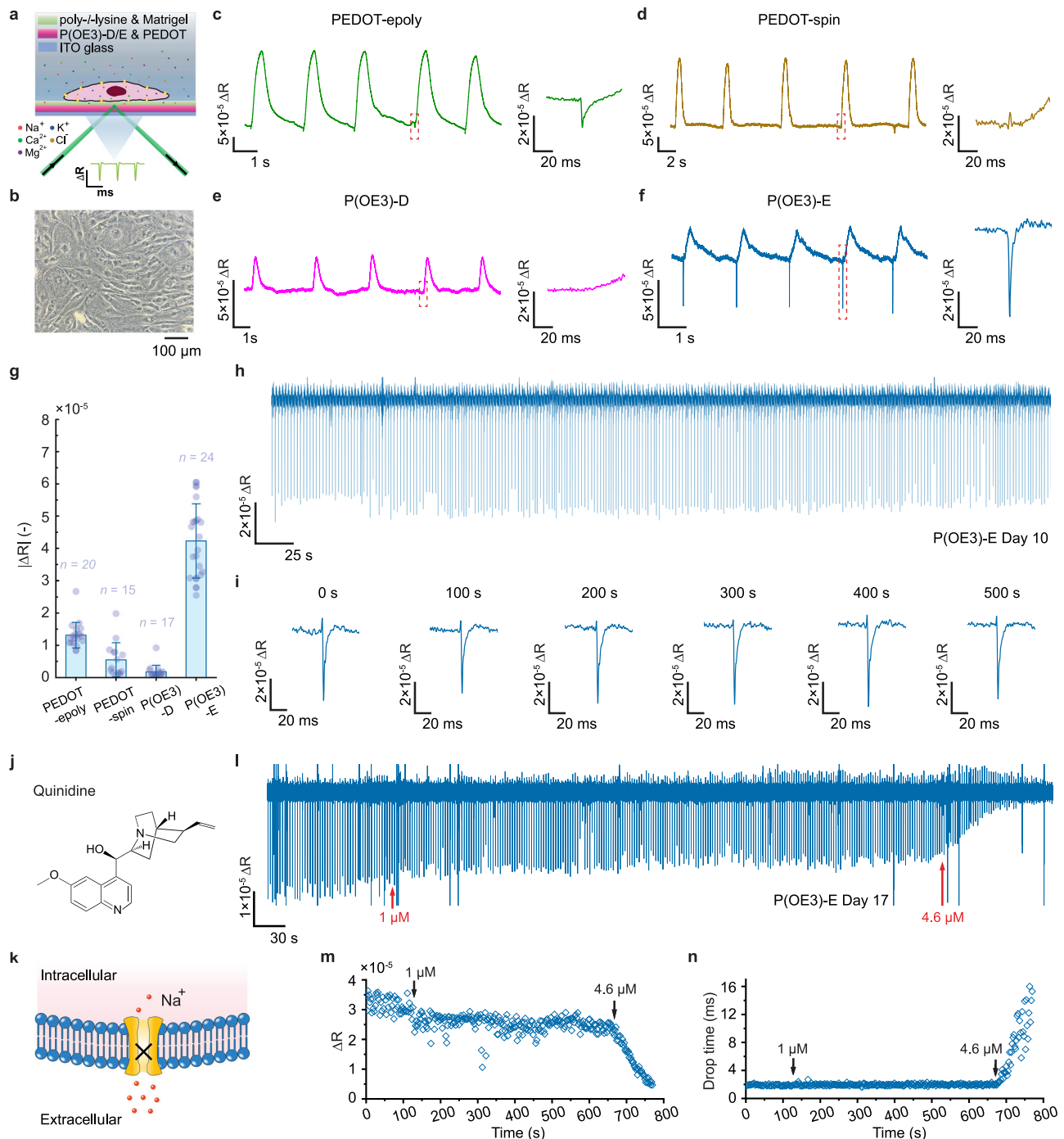


Fig. 4 | ECORE recording of hiPSC-cardiomyocyte action potentials using polymer thin films. **a** Schematic drawing of a hiPSC-cardiomyocyte cultured on top of electrochromic polymer thin films. **b** Optical micrograph of hiPSC-cardiomyocytes monolayer cultured on a P(OE3)-E thin film at day 10. The experiment was repeated independently with similar results at least 5 times. ECORE recording trace of a single hiPSC-cardiomyocyte 8 days after cell seeding using **c** PEDOT-epoly thin film, **d** PEDOT-spin thin film, **e** P(OE3)-D thin film, and **f** P(OE3)-E thin film. **g** Comparison of the recording performance for hiPSC-cardiomyocytes action potentials 7–10 days after cell seeding in terms of reflectance change, ΔR , using four polymers. Data are presented as mean \pm SD; $n = 20, 15, 17, 24$ cells for

PEDOT-epoly, PEDOT spin, P(OE3)-D, and P(OE3)-E films. **h** A 10-min recording trace of a single hiPSC-cardiomyocyte 10 days after cell seeding on a P(OE3)-E film at 10 kHz recording frequency. **i** Zoomed-in traces at 0, 100, 200, 300, 400, and 500 s show that the optical signal remains stable over the long recording period. **j**, **k** Quinidine as a voltage-gated sodium channel blocker. **l** A representative recording trace of a hiPSC-cardiomyocyte using P(OE3)-E when 1 and 4.6 μM of quinidine were added at indicated times during recording. Quantifications of **m** the extracellular action potential amplitude in terms of ΔR , and **n** the peak-to-valley time-scale as a function of time. The times of quinidine additions were noted on the trajectories.

high signal quality and reliability. These findings highlight the potential of P(OE3)-E and its derivatives for advancing bioelectronics. As ECORE is still a nascent technology, we envision a number of opportunities for further improvement. On the optical front, increasing spatial resolution by minimizing the probing laser spot size, and boosting recording

throughput via laser beam scanning, are promising avenues. From a materials perspective, developing materials with greater electrochromic contrast across various redox states, tailored for different biological environments, will be critical. Together, these advancements will drive ECORE toward becoming a versatile and powerful tool

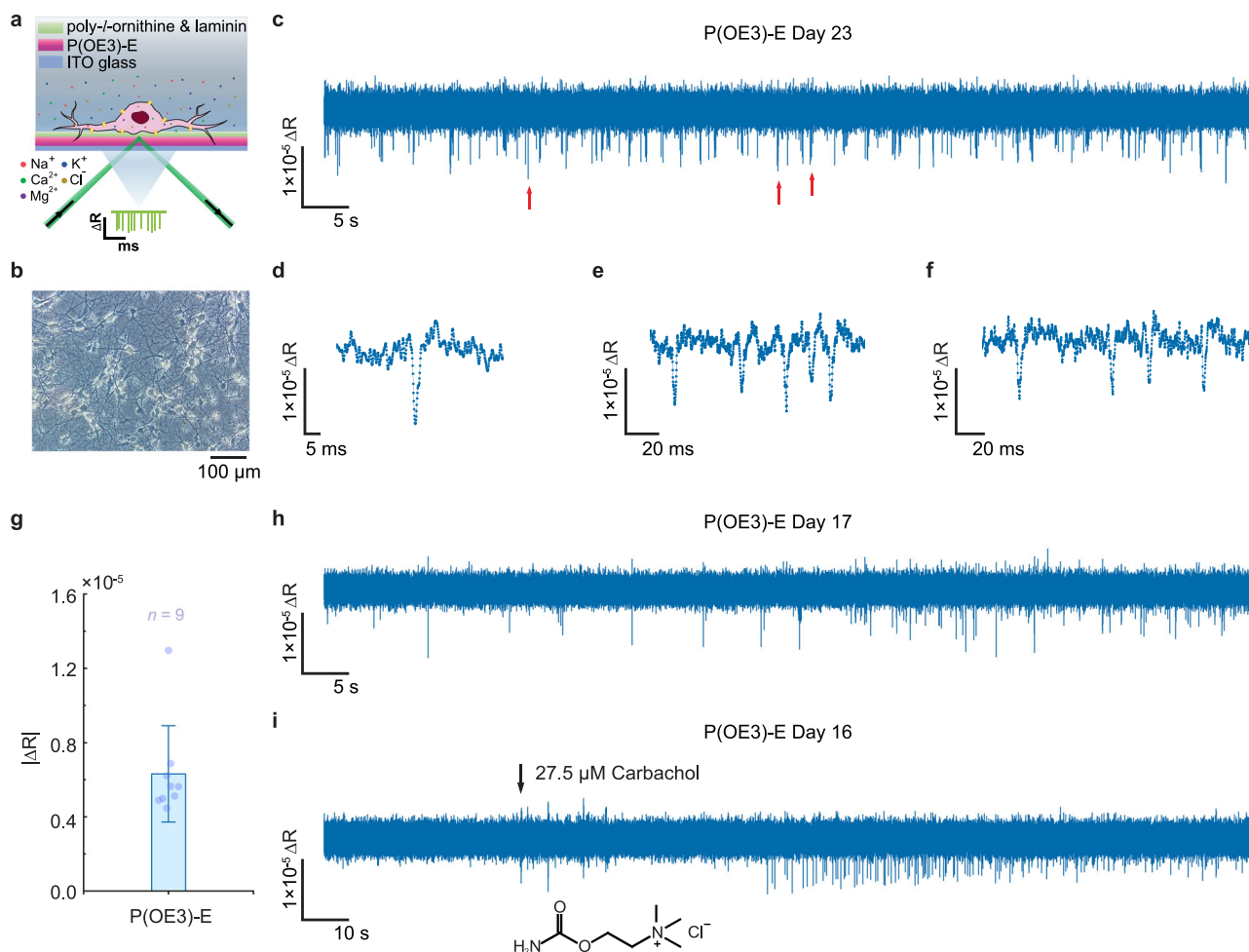


Fig. 5 | ECORE recording of neuronal action potentials using P(OE3)-E polymer thin films. **a** Schematic drawing of a rat hippocampal neuron cultured on top of a P(OE3)-E thin film. **b** Optical micrograph of dissociated rat hippocampal neurons cultured on a P(OE3)-E thin film on day 9. The experiment was repeated independently with similar results 5 times. **c** A 100-s ECORE recording trace of spontaneous neuronal action potentials using a P(OE3)-E thin film 23 days after cell seeding. **d** Zoomed-in view of a single neuronal action potential spike (1st red arrow in **c**) Inset: many data points are sampled for a single neuronal action potential spike.

e, f Zoomed-in views (2nd and 3rd red arrow in **c**) show neuronal burst firing. **g** Recording performance for neuronal action potentials in terms of reflectance change, ΔR , using P(OE3)-E thin films. Data are presented as mean \pm SD; $n = 9$ cells. **h** A 100-s ECORE recording trace of spontaneous neuronal action potentials 17 days after cell seeding on a P(OE3)-E thin film. **i** A 200-s ECORE recording trace of stimulated neuronal action potentials using carbachol 16 days after cell seeding on a P(OE3)-E thin film.

for detecting electrical and electrochemical signals in biological systems.

Methods

Materials and device fabrication

The synthesis of P(OE3)-D and P(OE3)-E was carried out by C-H direct (hetero)arylation polymerization and was previously reported¹⁷. The number-average molecular weight and dispersity were $M_n = 27$ kg/mol and $\bar{D} = 2.9$ for P(OE3)-D, and $M_n = 13$ kg/mol and $\bar{D} = 2.0$ for P(OE3)-E. Indium tin oxide (ITO) coated glass slides ($25 \times 25 \times 0.4$ mm³) with resistance $R_s = 70$ – 100Ω (Surplus Part No. X260, Delta Technologies) were first cleaned with dish soap in a sonicator bath for 5 min. They were then dried and cleaned using a UV-ozone cleaner (UV-1, Samco) at 60 °C for 4 min.

For P(OE3)-D and P(OE3)-E films, the four edges of the cleaned ITO coated glass were masked using vinyl electrical tapes (3M) leaving a center area of 12×12 mm². P(OE3)-D or P(OE3)-E were dissolved in chloroform with a concentration of 5 mg/mL and then spin-coated onto the ITO coated glass using a spin coater (WS-400B-6NPP/LITE, Laurell) at 1200 rpm or 1300 rpm. During spin coating, ~ 80 μ L solution was used through a dynamic

dispense technique for each device. After spin coating, the masking electrical tapes were carefully removed using a sharp tweezer. The substrate was then cleaned with chloroform using a Q-tip to remove any tape and polymer residues. A custom 3-D printed poly(lactic acid) (PLA) sample well with a circular bottom opening of $\varnothing 6$ mm was then glued onto the ITO-coated glass slide using RTV108 silicone glue (Momentive) and was allowed to cure for 48 h. Typically, five to six devices are prepared each time for each polymer.

For spin-coated PEDOT:PSS films (PEDOT-spin), 16 mL PEDOT:PSS dispersion (Clevios PH1000), 4 mL ethylene glycol (BDH1125-1LP, VWR Chemicals), 24 μ L sodium dodecylbenzenesulfonate (DBSA) (440167-100 ML, Sigma-Aldrich), and 200 μ L (3-glycidyloxypropyl)trimethoxysilane (GOPS) (D098925G, Fisher Scientific) were first vortex mixed followed by 5 min sonication. The solution was then filtered using 1.2 μ m cellulose acetate syringe filters (Sartorius). The mixed dispersion was spin-coated onto the ITO glass at 5800 rpm using a static dispense technique and annealed at 140 °C on a heat stage for at least 1 h. Finally, the custom 3-D printed PLA sample well was glued to the glass slide and allowed to cure for 48 h.

For electropolymerized PEDOT:PSS films (PEDOT-epoly), the custom 3-D printed PLA sample well was first glued to the cleaned ITO glass slide and allowed to cure for 48 h. Deionized (DI) water ($R = 18.2 \text{ m}\Omega/\text{cm}$) 19.58 mL was mixed with 0.4 g (2 w/w%) poly(sodium 4-styrenesulfonate) (PSS) ($M_w = 70,000$, Sigma-Aldrich) and 20 μL 3,4-ethylenedioxythiophene (EDOT) (483028, Sigma-Aldrich) to make a 10 mM solution. The solution was allowed to equilibrate overnight and filtered using a 1.2 μm cellulose acetate syringe filter (Sartorius). The mixed EDOT and PSS solutions were then added to the sample well for electropolymerization by controlling the voltage or charge, as detailed in our previous work¹⁴.

All spin-coated polymer thin film devices were electrochemically conditioned between -0.4 V and 0.3 V at 100 mV/s for 5 cycles in HEPES (4-(2-hydroxyethyl)-1-piperazineethanesulfonic acid) buffered Tyrode's salt solution and were stored in DI water for 24 h before all ECORE measurements.

UV-Vis-NIR spectroelectrochemistry

A polymer thin film sample coated on the ITO glass, an Ag/AgCl reference electrode (RE6, BASi Research Products), and a platinum counter electrode were placed in a custom-designed, 3-D printed cuvette and placed in the sample chamber of a UV-vis-NIR spectrophotometer (Lambda 365, PerkinElmer), as described before¹⁴. The position of the cuvette was adjusted such that the probing light beam passes through the center of the polymer film. The UV-vis-NIR spectrophotometer scans from 300 to 1100 nm with a 1 nm step. The aqueous electrolyte was HEPES buffered Tyrode's salt solution for all measurements. A potentiostat (SP-200, BioLogic) was used to apply the potential to all polymer films from $+600$ to -600 mV with a 100 mV step. The potential step changes from 100 to 50 mV between $+200$ and -200 mV for all polymer films. The lowest reducing potential was selected when all polymer films were fully driven into the reduced (dedoped) state.

The film thickness used for UV-Vis-NIR spectroelectrochemistry for P(OE3)-D, P(OE3)-E, and PEDOT-epoly was 67 nm, 70 nm, and 139 nm, respectively. Because of the low mass density of PEDOT in commercialized PEDOT:PSS dispersions, we cast a thicker film of 836 nm such that the minimum absorbance data could reach the detection limit of the spectrophotometer. To directly compare the UV-vis-NIR spectroelectrochemistry shift of all polymers at 561 nm, the absorbance value of the polymer films was normalized with respect to the peak absorbance value in the reduced state at -600 mV applied voltage.

Thickness and surface characterization of conjugated polymer thin films

A blunt tip tweezer was used to gently scratch near the center of the polymer thin films. The thickness of the polymer thin films was then measured using a Bruker Dektak XT profilometer (Bruker Corporation). For each sample, five measurements were performed, and the average film thickness was calculated. The surface morphology of the polymer films was imaged using a Bruker Dimension Icon atomic force microscope (AFM) (Bruker Corporation) under the peak force tapping mode using an NSC19/Al BS AFM probe (Mikromasch). The surface roughness of the film was calculated as the standard deviation of the AFM image over an $1 \mu\text{m}^2$ area using NanoScope Analysis 1.9 software (Bruker Corporation).

Color change of conjugated polymer thin films

The color change of all the polymer films is captured using a camera (iPhone 13, Apple Inc.) under the same light conditions in a photo studio light box. A potentiostat (SP-200, BioLogic) was used to apply different potentials to the polymer film and the aqueous electrolyte was HEPES buffered Tyrode's salt solution.

Optical setup of ECORE

A 50 mW, 561 nm diode-pumped solid-state laser (Excelsior, Spectra-Physics) was directed through a 0.3 (50%) and a 0.1 (79%) neutral density filter and coupled into a single mode optical fiber (P3-460B-FC-2, Thorlabs). The polarization of the two overlapping laser beams was then adjusted using an achromatic half-wave plate (AHWP05M-600, Thorlabs) and filtered by a polarizing beam splitter cube (PBS201, Thorlabs). The filtered beams were again directed through an 830 nm half-wave plate (WPH05M-830, Thorlabs) and an achromatic half-wave plate (AHWP05M-600, Thorlabs). A second polarized beam splitter cube (PBS101, Thorlabs) then separated the polarized probing beam into *p*- and *s*-polarized beam and the amount of *p*- and *s*-polarization was manually controlled by the preceding two half-wave plates. The sample beam was directed through a third achromatic half-wave plate (AHWP10M-600, Thorlabs) and the beam was adjusted to *s*-polarization and focused to the prism. A 20 mm BK-7 equilateral prism (24-2158-000, Ealing Catalog) was placed on a custom 3-D printed prism holder mounted to a rotational stage (CR1, Thorlabs) and the laser incident angle can be tuned adjusting the prism angle. The rotational stage was mounted on an XYZ linear translational stage (9064-XYZ, Newport) so that the position of the prism can also be adjusted. The collected sample beam and the reference beam were directed to a differential photodetector. By detecting the reflected light, we avoid spurious signals resulting from light scattering from cells or the lipid–air interface¹⁵. The upper surface of the sample can also be kept free for imaging and inserting electrodes for calibration. Differential photodetection could reduce common-mode fluctuations such as vibrations or noise due to laser intensity instabilities. A 20 \times objective (LMPlanFI, Olympus) connected to a CCD camera (GS3-U3-23S6M-C, Teledyne FLIR) was mounted on top of the prism for brightfield imaging of the sample well and location of the probing laser spot. The size of the probing laser spot was characterized to be $\sim 25 \mu\text{m}$. More details regarding the ECORE setup were described in our previous work¹⁴.

Isolated rat embryonic heart culture

Whole rat hearts were isolated from embryonic day 18 (E18) Sprague Dawley rat embryos (Charles River Laboratories) and all blood vessels were removed with a fine tweezer under a dissection microscope in HHBSS dissection medium (Hanks' Balanced Salt Solution, Gibco; +10 mM HEPES, pH = 7.4, Gibco). Isolated hearts were washed three times with HHBSS dissection medium and cultured in suspension in RPMI 1640 medium (REF 11875-093, 500 mL, Gibco) with 1 \times B-27 supplement (REF 17504-044, 10 mL, Gibco). The medium was changed to fresh medium every 2–3 days. The embryonic hearts will beat for a few minutes to 1 h in vitro right after the dissection, and then turn silent for around a week before restarting to beat again. Beating activities resume in $\sim 60\%$ of the hearts after 1–2 weeks and will last for months in the culture dish. The optical micrograph of the E18 rat heart was captured using a camera (iPhone 13, Apple Inc.) through the eyepiece of an inverted phase contrast tissue culture microscope under a 5 \times objective (DMI1, Leica).

HiPSC-cardiomyocyte culture

The devices with different polymer thin films were first disinfected with 70% EtOH for 30 min. After rinsing with 1 \times phosphate-buffered saline (PBS) solution (21-040-CM, Corning) for three times, the polymer film was coated with 1 mg/mL poly-L-lysine (10 \times) in PBS for 30 min, followed by PBS rinsing for three times. The polymer film was then coated with 0.5% glutaraldehyde in PBS for 15 min, followed by another three-time PBS rinsing. Everything up to this point took place at room temperature. Next, the polymer film was coated with 1:200 Matrigel (REF 35623, Corning) in DMEM/F12 (REF 10565-018, Gibco) at 37°C for 1 h.

HiPSC-derived cardiomyocytes were maintained in Matrigel pre-coated 6-well plates in RPMI 1640 media (REF 11875-093, 500 mL,

Gibco) with 1× B-27 supplement (REF 17504-044, 10 mL, Gibco). The culture media was refreshed every 2–3 days. To transfer cells onto the devices with polymer thin films, cardiomyocytes were first dissociated with TryPLE select 10× (REF A12177-01, Gibco) at 37 °C for 5 min from the 6-well plate, then $\sim 1.2 \times 10^5$ cells were plated in each coated polymer device in RPMI 1640 media with 1× B-27 supplement and 10% KnockOut Serum Replacement (KSR) (REF A31815-01, Gibco). The devices with cells are then cultured in a 5% CO₂ incubator at 37 °C. The media was changed to RPMI 1640 media with 1× B-27 supplement the second day after cell seeding and refreshed every 2 days. The cardiomyocytes cultured on the polymer films exhibit spontaneous and rhythmic contractions 2–3 days after seeding and ECORE recordings start a week after cell seeding. These devices with cardiomyocytes can be maintained on the polymer thin films for months of time. The optical micrograph of the hiPSC-cardiomyocytes was captured using a camera (iPhone 13, Apple Inc.) through the eyepiece of an inverted phase contrast tissue culture microscope under a 20× objective (DMI1, Leica).

Dissociated rat hippocampal neuron culture

The devices with P(OE3)-E thin films were first disinfected with 70% EtOH for 30 min. After rinsing with 1× PBS solution for three times, the polymer film was coated with 50 µg/mL poly-L-ornithine (P3655, Sigma-Aldrich) in PBS for 2 h at 37 °C, followed by PBS rinsing for three times. The polymer film was then coated with 2.5 µg/mL laminin (CC160-350UG, Millipore) in PBS and stored in a 37 °C incubator overnight.

Rat hippocampal neurons were extracted from embryonic day 18 (E18) Sprague Dawley rat embryos. The rat hippocampus were first isolated from E18 rat brains using a fine tweezer in HHBSS dissection medium (Hanks' Balanced Salt Solution, Gibco; +10 mM HEPES, pH = 7.4, Gibco) on ice under a dissection microscope. Isolated rat hippocampi were rinsed 12 times with HHBSS dissection medium. TryPLE Select (1×) (REF 12563-011, 100 mL, Gibco) with 80 µg/mL DNase I was used for gentle enzymatic digestion of the extra tissue in the hippocampi. After 30 min enzymatic digestion, the neurons were resuspended in 1 mL of plating medium containing Neurobasal (REF 21103-049, 500 mL, ThermoFisher), 2 mM GlutaMAX (REF 35050-061, 100 mL, Gibco), 1× B-27 (REF 17504-044, 10 mL, Gibco), and 10% FBS and filtered using 100 µm nylon mesh. For each dissection, 8 hippocampi from 4 E18 rat brains were dissected and ~ 1.5 –2 million cells can be harvested.

The laminin in the device was then removed and the cell plating medium is added to the device with a cell density of ~ 1400 cells/mm². After cell seeding, a custom 3-D printed cap covered with fluorinated ethylene propylene (FEP) film was capped to the sample well to prevent cell medium evaporation but still allowed for gas exchange with the environment. The devices seeded with neurons were cultured in a 5% CO₂ incubator at 37 °C. All the cell plating medium was changed to growth medium I containing Neurobasal, 2 mM GlutaMAX, 1× B-27, and 1% FBS the next day after seeding. After 3–4 days, 1/2 of the growth medium was changed to growth medium II containing Neurobasal, 2 mM GlutaMAX, and 1× B-27. After another 3–4 days, 1/3 of the medium was refreshed with growth medium II. No medium change or one more 1/3 medium change of growth medium II was needed afterwards, depending on the health condition of the neurons. The neurons can be kept in culture on P(OE3)-E film for over 3 weeks. The optical micrograph of the neurons was captured using a camera (iPhone 13, Apple Inc.) through the eyepiece of an inverted phase contrast tissue culture microscope under a 20× objective (DMI1, Leica).

ECORE data acquisition

For ECORE recording of cell electrical signals, the cell culture media was replaced with 200 µL of HEPES buffered Tyrode's solution at 37 °C

before each measurement. For ECORE recording of isolated rat hearts, the polymer film was first coated with 0.1 mg/mL poly-D-lysine for 30 min followed by PBS rinsing for three times. The rat heart culture dish was examined under the dissection microscope using a 5× objective and a beating heart was chosen. The selected rat heart was then transferred from the culture dish onto the polymer film using a cutted 1000 µL pipette tip. The position of the heart was adjusted to the center of the device. The heart culture medium was then carefully removed and replaced with 200–300 µL HEPES buffered Tyrode's solution at 37 °C. The rat heart will “stick” to the polymer film over time.

Next, a thin layer of Type F immersion oil ($n_0 = 1.518$, Leica) was applied to the bottom of the device for index matching with the prism and suppression of back reflection from the ITO glass. The 561 nm probing laser was focused on the location of interest on the isolated rat heart or the cell of interest. The sample and the reference beams were directed to the two photodiodes of the homemade differential photodiode detector, which convert optical signals from the probing laser into voltage signals. The voltage output from the differential photodetectors was filtered using a 10 kHz low-pass electrical filter (EF120, Thorlabs) and amplified through a patch clamp amplifier (Axopatch-1A, Molecular Devices). The amplified output from the amplifier was connected to an 8 kHz homemade Bessel filter to filter out the amplifier noise. The filtered, amplified signal was then digitized at 10 kHz rate using a low-noise digitizer (Axon Digidata 1440 A, Molecular Devices) and recorded using c software. The light intensities of the sample beam and the reference beam reaching the differential photodetectors were manually adjusted by rotating an achromatic half-wave plate in the light path. The differential photodetector was therefore ‘balanced’ to maximize the recording dynamic range for reflectance change ΔR (in Volts). The power of the incident probing laser beam (in mW) reaching the sample was measured using a photodiode power sensor (S121C, Thorlabs) connected to an optical power meter (PM100D, Thorlabs).

Pharmacology experiments

Quinidine (Q3625, Sigma-Aldrich) and carbachol (PHR1511, Sigma-Aldrich) were dissolved in dimethyl sulfoxide (DMSO) to make 100 mM and 50 mM stock solutions, respectively. Quinidine and carbachol were diluted in HEPES buffered Tyrode's solution to 20 and 100 µM warmed to 37 °C. For all experiments, 200 µL of HEPES buffered Tyrode's solution already exists in the sample well. For cardiomyocyte recording, 60 µL of 20 µM quinidine was carefully added into the sample well using a pipette, yielding a final drug concentration of 4.6 µM. For neuron recording, 76 µL of 100 µM carbachol was carefully added into the sample well using a pipette, yielding a final drug concentration of 27.5 µM.

Data analysis

The reflectance change ΔR of the polymer film was normalized with respect to the incident probing laser beam power reaching the sample P_{in} (in mW). Since the photodiode converts light into electrical signal, the reflectance change ΔR is defined as

$$\Delta R[-] = \frac{\text{Recorded signal [Volts]}}{(\text{responsivity [A/W]} \times \text{feedback resistance } [\Omega] \times \text{incident laser power [W]} \times \text{amplifier gain [-]})} \quad (1)$$

The responsivity varies depending on the photodiode material and the laser wavelength. The responsivity is 0.232 A/W for the silicon photodiode (FDS100, Thorlabs) used in the differential photodetector at 561 nm. The feedback resistor resistance in the differential photodetector is 100 kΩ. The amplifier gain was set to 50× for cell-free squarewave potential recordings and 100× for biological recordings.

For squarewave potential recordings, electrical noise with reference frequency of 60 Hz was filtered to the 10th harmonics (3 dB bandwidth of 0.72 Hz) using Clampfit 11. A 3rd order Butterworth low-pass filter (cutoff frequency of 500 Hz) and a 1st order Butterworth high-pass filter (cutoff frequency of 0.2 Hz) were then applied using Python. For rat heart and cardiomyocyte recordings, electrical noise with reference frequency of 60 Hz was filtered to the 10th harmonics (3 dB bandwidth of 0.72 Hz) and an 8-pole Butterworth low-pass filter (cutoff frequency of 500 Hz) was applied using Clampfit 11. A 1st order Butterworth high-pass filter (cutoff frequencies between 0.1 and 2 Hz) was also applied using Python to flatten the recording baseline shift. For neuronal recordings, electrical noise with reference frequency of 60 Hz was filtered to the 20th harmonics (3 dB bandwidth of 0.36 Hz), a bandpass filter between 50 Hz (single-pole RC high-pass filter) and 1000 Hz (8-pole Butterworth low-pass filter) was then applied using Clampfit 11. The recording baseline noise was determined by the standard deviation of a 25 ms baseline that is relatively flat before the action potential spikes.

Custom codes in Python were used to determine the height of the squarewave potentials, the action potential spikes, and the full rise or drop (baseline-to-peak) timescales of single-phasic and bi-phasic spikes. The average ΔR for square wave potentials was calculated as the average step height over 60 s (≥ 5 square waves). The average ΔR for action potentials was calculated as the average spike height over 40–400 s depending on the firing frequency of the tissue/cell (≥ 40 spikes).

Ethics

IPSCs were obtained from Stanford Cardiovascular Institute Biobank and used per Institutional Review Board/Stem Cell Research Oversight Panel guidelines, adhering to federal, state, and Stanford University human stem cell research policies. The use of laboratory rats was approved by the Stanford University Administrative Panel on Laboratory Animal Care and adhered to relevant ethical regulations.

Reporting summary

Further information on research design is available in the Nature Portfolio Reporting Summary linked to this article.

Data availability

All data supporting the findings of this study are available within the article and its supplementary files. Any additional requests for information can be directed to, and will be fulfilled by, the corresponding authors. Source data are provided with this paper.

Code availability

The custom Python code used in this study is available from GitHub (<https://github.com/zlab798/25NatCommDataAnalysis>).

References

- Paulsen, B. D., Tybrandt, K., Stavrinidou, E. & Rivnay, J. Organic mixed ionic-electronic conductors. *Nat. Mater.* **19**, 13–26 (2020).
- Paulsen, B. D., Fabiano, S. & Rivnay, J. Mixed ionic-electronic transport in polymers. *Annu. Rev. Mater. Res.* **51**, 73–99 (2021).
- Bryan, A. M., Santino, L. M., Lu, Y., Acharya, S. & D'Arcy, J. M. Conducting polymers for pseudocapacitive energy storage. <https://doi.org/10.1021/acs.chemmater.6b01762> (2016).
- Österholm, A. M., Ponder, J. F. Jr, Kerszulis, J. A. & Reynolds, J. R. Solution processed PEDOT analogues in electrochemical supercapacitors. *ACS Appl. Mater. Interfaces* **8**, 13492–13498 (2016).
- Li, X., Li, Y., Sarang, K., Lutkenhaus, J. & Verduzco, R. Side-chain engineering for high-performance conjugated polymer batteries. *Adv. Funct. Mater.* **31**, 2009263 (2021).
- Das, P. et al. Enhancing the ionic conductivity of poly(3,4-propylenedioxythiophenes) with oligoether side chains for use as conductive cathode binders in lithium-ion batteries. *Chem. Mater.* <https://doi.org/10.1021/acs.chemmater.1c03971> (2022).
- Liang, Y., Offenhäusser, A., Ingebrandt, S. & Mayer, D. PEDOT:PSS-based bioelectronic devices for recording and modulation of electrophysiological and biochemical cell signals. *Adv. Healthc. Mater.* **10**, 2100061 (2021).
- Liu, J. et al. Intrinsically stretchable electrode array enabled in vivo electrophysiological mapping of atrial fibrillation at cellular resolution. *Proc. Natl. Acad. Sci. USA* **117**, 14769–14778 (2020).
- Keene, S. T. et al. A biohybrid synapse with neurotransmitter-mediated plasticity. *Nat. Mater.* **19**, 969–973 (2020).
- Liu, Y. et al. Soft conductive micropillar electrode arrays for biologically relevant electrophysiological recording. *Proc. Natl. Acad. Sci. USA* **115**, 11718–11723 (2018).
- Williams, J. C., Hippensteel, J. A., Dilgen, J., Shain, W. & Kipke, D. R. Complex impedance spectroscopy for monitoring tissue responses to inserted neural implants. *J. Neural Eng.* **4**, 410–423 (2007).
- Khodagholy, D. et al. NeuroGrid: recording action potentials from the surface of the brain. *Nat. Neurosci.* **18**, 310–315 (2014).
- Jacobs, I. E. et al. High-efficiency ion-exchange doping of conducting polymers. *Adv. Mater.* **34**, e2102988 (2022).
- Zhou, Y. et al. Dual-color optical recording of bioelectric potentials by polymer electrochromism. *J. Am. Chem. Soc.* **144**, 23505–23515 (2022).
- Alfonso, F. S. et al. Label-free optical detection of bioelectric potentials using electrochromic thin films. *Proc. Natl. Acad. Sci. USA* **117**, 17260–17268 (2020).
- Savagian, L. R. et al. Balancing charge storage and mobility in an oligo(Ether) functionalized dioxothiophene copolymer for organic- and aqueous-based electrochemical devices and transistors. *Adv. Mater.* **30**, e1804647 (2018).
- Advincula, A. A. et al. Probing comonomer selection effects on dioxothiophene-based aqueous-compatible polymers for redox applications. *Chem. Mater.* **34**, 4633–4645 (2022).
- Ponder, J. F. Jr, Österholm, A. M. & Reynolds, J. R. Designing a Soluble PEDOT analogue without surfactants or dispersants. *Macromolecules* **49**, 2106–2111 (2016).
- Advincula, A. A. et al. Elucidating design rules toward enhanced solid-state charge transport in oligoether-functionalized dioxothiophene-based alternating copolymers. *ACS Appl. Mater. Interfaces* <https://doi.org/10.1021/acsami.3c00053> (2023).
- Jones, A. L. et al. Branched oligo(ether) side chains: a path to enhanced processability and elevated conductivity for polymeric semiconductors. *Adv. Funct. Mater.* **31**, 2102688 (2021).
- Gribkova, O. L. et al. The influence of polyacid nature on poly(3,4-ethylenedioxythiophene) electrosynthesis and its spectro-electrochemical properties. *J. Solid State Electrochem.* **20**, 2991–3001 (2016).
- Kabanova, V., Gribkova, O. & Nekrasov, A. Poly(3,4-ethylenedioxythiophene) electrosynthesis in the presence of mixtures of flexible-chain and rigid-chain polyelectrolytes. *Polymers* **13**, 3866 (2021).
- Marzocchi, M. et al. Physical and electrochemical properties of PEDOT:PSS as a tool for controlling cell growth. *ACS Appl. Mater. Interfaces* **7**, 17993–18003 (2015).
- Koutsouras, D. A. et al. Impedance spectroscopy of spin-cast and electrochemically deposited PEDOT:PSS films on microfabricated electrodes with various areas. *ChemElectroChem* **4**, 2321–2327 (2017).
- Bers, D. M. Cardiac excitation–contraction coupling. *Nature* **415**, 198–205 (2002).
- Xie, C., Lin, Z., Hanson, L., Cui, Y. & Cui, B. Intracellular recording of action potentials by nanopillar electroporation. *Nat. Nanotechnol.* **7**, 185–190 (2012).
- Patlak, J. B. & Ortiz, M. Slow currents through single sodium channels of the adult rat heart. *J. Gen. Physiol.* **86**, 89–104 (1985).

28. Brown, A. M., Lee, K. S. & Powell, T. Sodium current in single rat heart muscle cells. *J. Physiol.* **318**, 479–500 (1981).
29. Yang, Y. et al. Cardiotoxicity drug screening based on whole-panel intracellular recording. *Biosens. Bioelectron.* **216**, 114617 (2022).
30. Spira, M. E. & Hai, A. Multi-electrode array technologies for neuroscience and cardiology. *Nat. Nanotechnol.* **8**, 83–94 (2013).
31. Gold, C., Henze, D. A., Koch, C. & Buzsáki, G. On the origin of the extracellular action potential waveform: a modeling study. *J. Neurophysiol.* **95**, 3113–3128 (2006).
32. Suresh, J. et al. Network burst activity in hippocampal neuronal cultures: the role of synaptic and intrinsic currents. *J. Neurophysiol.* **115**, 3073–3089 (2016).
33. Semple, B. D., Blomgren, K., Gimlin, K., Ferriero, D. M. & Noble-Haeusslein, L. J. Brain development in rodents and humans: Identifying benchmarks of maturation and vulnerability to injury across species. *Prog. Neurobiol.* **106–107**, 1–16 (2013).
34. Miyazawa, A., Fujiyoshi, Y. & Unwin, N. Structure and gating mechanism of the acetylcholine receptor pore. *Nature* **423**, 949–955 (2003).
35. Kruse, A. C. et al. Structure and dynamics of the M3 muscarinic acetylcholine receptor. *Nature* **482**, 552–556 (2012).
36. Robert, V. et al. The mechanisms shaping CA2 pyramidal neuron action potential bursting induced by muscarinic acetylcholine receptor activation. *J. Gen. Physiol.* **152**, e201912462 (2020).
37. Zhou, Y., Liu, E., Müller, H. & Cui, B. Optical electrophysiology: toward the goal of label-free voltage imaging. *J. Am. Chem. Soc.* **143**, 10482–10499 (2021).
38. Kiskinis, E. et al. All-optical electrophysiology for high-throughput functional characterization of a human iPSC-derived motor neuron model of ALS. *Stem Cell Rep.* **10**, 1991–2004 (2018).
39. Hochbaum, D. R. et al. All-optical electrophysiology in mammalian neurons using engineered microbial rhodopsins. *Nat. Methods* **11**, 825–833 (2014).
40. Adam, Y. All-optical electrophysiology in behaving animals. *J. Neurosci. Methods* **353**, 109101 (2021).
41. Ponder, J. F. et al. Conductive, solution-processed dioxythiophene copolymers for thermoelectric and transparent electrode applications. *Adv. Energy Mater.* **9**, 1900395 (2019).

Acknowledgements

The authors thank Professor Steven Boxer for the access of the patch clamp digitizer and UV-vis-NIR spectrophotometer in his lab, and Jacob Kirsh for helping with the UV-vis-NIR spectrophotometer training. The authors thank Professor Joseph C. Wu for providing the hiPSC-cardiomyocytes cell line. The authors thank Dr. Fuu-Jiun Hwang and Professor Jun Ding for inspiring discussions on neuroelectrophysiology. This work was financially supported by the National Institutes of Health grant No. R01NS121934 and the Office of Naval Research N00014-22-1-2185. E.L. acknowledges the NIH Stanford Graduate Training Program in Biotechnology T32GM141819 and the Stanford Bio-X Bowes Fellowship. Part of this work was performed at the Stanford

Nano Shared Facilities (SNSF), supported by the National Science Foundation under award ECCS-2026822.

Author contributions

Y.Z. and B.C. conceived of the study and designed the experiments. Y.Z., E.L., and P.S. performed the ECORE experiments. A.M.Ö. and A.L.J. synthesized and characterized P(OE3)-D and P(OE3)-E polymers. Y.Y. and W.Z. contributed to the cell culture and dissection experiments. C.-T.T. contributed to the AFM measurements. T.Z. contributed to developing the data analysis code. Y.Z., H.M., J.R.R. and B.C. discussed the results and wrote the paper with feedback from all authors.

Competing interests

The authors declare no competing interests.

Additional information

Supplementary information The online version contains supplementary material available at <https://doi.org/10.1038/s41467-025-61708-y>.

Correspondence and requests for materials should be addressed to Bianxiao Cui.

Peer review information *Nature Communications* thanks Shiguo Zhang and the other, anonymous, reviewer for their contribution to the peer review of this work. A peer review file is available.

Reprints and permissions information is available at <http://www.nature.com/reprints>

Publisher's note Springer Nature remains neutral with regard to jurisdictional claims in published maps and institutional affiliations.

Open Access This article is licensed under a Creative Commons Attribution-NonCommercial-NoDerivatives 4.0 International License, which permits any non-commercial use, sharing, distribution and reproduction in any medium or format, as long as you give appropriate credit to the original author(s) and the source, provide a link to the Creative Commons licence, and indicate if you modified the licensed material. You do not have permission under this licence to share adapted material derived from this article or parts of it. The images or other third party material in this article are included in the article's Creative Commons licence, unless indicated otherwise in a credit line to the material. If material is not included in the article's Creative Commons licence and your intended use is not permitted by statutory regulation or exceeds the permitted use, you will need to obtain permission directly from the copyright holder. To view a copy of this licence, visit <http://creativecommons.org/licenses/by-nc-nd/4.0/>.

© The Author(s) 2025